

Analysis of the ${}^3\text{He}(\alpha, \gamma){}^7\text{Be}$ and ${}^3\text{H}(\alpha, \gamma){}^7\text{Li}$ astrophysical direct capture reactions in a modified potential-model approach

E.M. Tursunov,^{1,*} S.A. Turakulov,^{1,†} and A.S. Kadyrov^{2,‡}

¹*Institute of Nuclear Physics, Academy of Sciences,
100214, Ulugbek, Tashkent, Uzbekistan*

²*Curtin Institute for Computation and Department of Physics and Astronomy,
Curtin University, GPO Box U1987, Perth, WA 6845, Australia*

Abstract

Astrophysical S factors and reaction rates of the direct radiative capture processes ${}^3\text{He}(\alpha, \gamma){}^7\text{Be}$ and ${}^3\text{H}(\alpha, \gamma){}^7\text{Li}$, as well as the primordial abundance of the ${}^7\text{Li}$ element, are estimated in the framework of a modified two-body potential model. It is shown that suitable modification of phase-equivalent α - ${}^3\text{He}$ potentials in the d waves can improve the description of the astrophysical S factor for the direct ${}^3\text{He}(\alpha, \gamma){}^7\text{Be}$ radiative capture reaction at energies above 0.5 MeV. An estimated ${}^7\text{Li}/\text{H}$ abundance ratio of $(4.89 \pm 0.18) \times 10^{-10}$ is in very good agreement with the recent measurement of $(5.0 \pm 0.3) \times 10^{-10}$ by the LUNA collaboration.

PACS numbers:

*Electronic address: tursune@inp.uz

†Electronic address: turakulov@inp.uz

‡Electronic address: a.kadyrov@curtin.edu.au

I. INTRODUCTION

Realistic estimation of the primordial abundances of the lithium isotopes ${}^6\text{Li}$ and ${}^7\text{Li}$, the two heaviest elements in Big Bang nucleosynthesis (BBN), is one of the most important and unsolved problems of nuclear astrophysics. The primordial abundances of these elements can be extracted from an analysis of astronomical observations of old metal-poor halo stars. For the ${}^7\text{Li}$ abundance astronomical data provide a value of ${}^7\text{Li}/\text{H}=(1.58^{+0.35}_{-0.28}) \times 10^{-10}$ [1] which is 2 to 4 times less than an estimate of ${}^7\text{Li}/\text{H}=(4.68\pm 0.67)\times 10^{-10}$ of the BBN model [2]. On the other hand, there is the so-called second lithium problem which is related to the abundance ratios of the lithium isotopes. A recent analysis of the direct measurements data of the LUNA collaboration yielded a value ${}^6\text{Li}/{}^7\text{Li} = (1.6 \pm 0.3) \times 10^{-5}$ [3] which is 3 orders of magnitude lower than the astronomical observation [4]. These problems were subjects of intense discussions during a recent topical workshop [5]. This demonstrates that they are still far from being solved.

An important question is whether or not the lithium problems originate from astronomy or nuclear physics. From one side a small primordial abundance of the ${}^6\text{Li}$ element is well described in nuclear physics from both experimental and theoretical perspectives. This element was mainly produced during the BBN epoch via the direct capture $d(\alpha, \gamma){}^6\text{Li}$ process. Until recently the main problem in theoretical studies of this process was connected with a consistent description of the isospin-forbidden E1 transition. Finally, results of theoretical calculations within the most realistic three-body model [6–9] are now in very good agreement with the direct data of the LUNA collaboration [3, 10]. Good agreement was obtained for all observable of practical interest including astrophysical S factor, reaction rates and the primordial abundance of the ${}^6\text{Li}$ element. The absolute values and temperature dependence of the reaction rates of the LUNA data have been reproduced with a good accuracy, which was a consequence of the correct treatment of the isospin-forbidden E1 transition in contrast to two-body models based on so-called exact-mass prescription [9, 11]. The calculated value of $(0.67 \pm 0.01) \times 10^{-14}$ [8, 9] for the ${}^6\text{Li}/\text{H}$ primordial abundance ratio is consistent with the estimate $(0.80 \pm 0.18) \times 10^{-14}$ of the LUNA collaboration [3].

The ${}^7\text{Li}$ isotope was produced mainly through radiative capture reactions ${}^3\text{He}(\alpha, \gamma){}^7\text{Be}$ and ${}^3\text{H}(\alpha, \gamma){}^7\text{Li}$ during the BBN period [12]. These direct capture reactions play a significant role also in stellar nucleosynthesis [13], as well as in the pp chain of solar hydrogen burning

[14]. The primordial abundance of the ${}^7\text{Li}$ element is evaluated from the reaction rates of the two capture processes mentioned above. The ${}^7\text{Be}$ nucleus is produced in the ${}^3\text{He}(\alpha, \gamma){}^7\text{Be}$ direct capture process and subsequently decays through electron capture resulting in the ${}^7\text{Li}$ element. The ${}^3\text{H}(\alpha, \gamma){}^7\text{Li}$ process then gives a small additional contribution to the lithium primordial abundance.

In recent years, the lithium abundance problem was discussed extensively from both experimental and theoretical viewpoints [2, 15]. One has to note that experimental measurements of these reactions in low-energy region face serious difficulties due to strong Coulomb repulsion. Nevertheless, direct data for the astrophysical S factor of the ${}^3\text{He}(\alpha, \gamma){}^7\text{Be}$ capture process at several energies around 100 keV were obtained by the LUNA collaboration in the underground facility [16, 17]. Later, this data set was supplemented with a more accurate value of the astrophysical S factor at Gamow peak energy region, $S_{34}(23_{-5}^{+6} \text{ keV})=0.548 \pm 0.054 \text{ keV}$, determined on the basis of observed neutrino fluxes from the Sun within the standard solar model [18]. Based on those results, the authors of Ref. [18] extracted an estimate of 5.0×10^{-10} for the ${}^7\text{Li}/\text{H}$ abundance, close to the standard BBN value and more than three times larger than the astronomical data. Recently, the astrophysical S factor was reevaluated at the solar Gamow energy peak and its value, $S_{34}(23_{-5}^{+6} \text{ keV})=0.590 \pm 0.050 \text{ keV b}$, overlaps with the previous estimate within the error bars [19]. Additionally, the data set for the reaction ${}^3\text{He}(\alpha, \gamma){}^7\text{Be}$ was recently extended up to 4.5 MeV in the center-of-mass frame energy [20, 21].

Theoretically, the astrophysical capture processes ${}^3\text{He}(\alpha, \gamma){}^7\text{Be}$ and ${}^3\text{H}(\alpha, \gamma){}^7\text{Li}$ have been studied in potential [22–25] and microscopic models [26–29], a microscopic R-matrix approach [30], as well as in a semimicroscopic phenomenological approach [31], a fermionic molecular dynamics (FMD) method [32] and a no-core shell model with continuum (NC-SMC) [33, 34]. The most realistic microscopic approaches [29, 32–34] still have problems with simultaneous description of the above mirror capture reactions, including the both absolute values and energy dependence of the astrophysical S factor.

In Ref. [22] a realistic potential model was developed for the description of the capture reactions mentioned above. It was shown that the potential model is able to describe the astrophysical S factors at low energies, below 0.5 MeV, which include the BBN energy region of $E_{\text{cm}}=180\text{--}400 \text{ keV}$, leading to good agreement with the experimental data [16–18]. However, the existing data sets at intermediate energies are underestimated and this

discrepancy increases with the energy. An important question is, whether the potential model can describe the astrophysical S factor of the direct capture processes ${}^3\text{He}(\alpha, \gamma){}^7\text{Be}$ and ${}^3\text{H}(\alpha, \gamma){}^7\text{Li}$ at low and intermediate energies simultaneously. Answering this question may have important implications for both nuclear theory and astrophysical applications.

The aim of the present study is to describe the existing data for the astrophysical S factors of the ${}^3\text{He}(\alpha, \gamma){}^7\text{Be}$ and ${}^3\text{H}(\alpha, \gamma){}^7\text{Li}$ direct capture reactions at low- and intermediate-energy regions and to estimate the reaction rates of these processes and the primordial abundance of the ${}^7\text{Li}$ element in the potential model. As it is known from the literature [22], the dipole E1-transition operator yields the main contribution to the above processes at low and intermediate energies. The E2 transition contributes only in the resonance energy region near 3 MeV in the center-of-mass frame. The M1 transition is even more suppressed and this is the case at all energies.

As it was shown in Ref. [22], below 0.5 MeV the main contribution to the E1 S factor comes from the initial $\alpha + {}^3\text{He}$ and $\alpha + {}^3\text{H}$ s -wave scattering states. However, at intermediate energies the role of the d -wave scattering states increases and their contribution becomes dominant beyond 2 MeV. On this basis it would be very useful to search for optimal d -wave $\alpha + {}^3\text{He}$ and $\alpha + {}^3\text{H}$ potentials, which would allow to better describe the astrophysical S factor data for the aforementioned capture reactions. In this way we perform an optimization procedure among phase equivalent $\alpha + {}^3\text{He}$ potentials in the partial $d_{3/2}$ and $d_{5/2}$ waves.

The two-body Gaussian potentials [23] will be examined. In Ref. [22] the potential parameters in the s wave were adjusted to reproduce the astrophysical S factor of the $\alpha + {}^3\text{He}$ direct capture reaction at low energies in addition to the phase shift data. In the $p_{3/2}$ and $p_{1/2}$ partial waves the potential parameters were additionally adjusted to reproduce the bound state properties: binding energies and the values of the asymptotic normalization coefficients (ANC) for the ${}^7\text{Be}(3/2^-)$ ground and ${}^7\text{Be}(3/2^-)$ excited states extracted from the analysis of the experimental data within the DWBA method [35].

This article is organized as follows. In Section II the theoretical model will be briefly described, Section III is devoted to the analysis of numerical results. Conclusions will be drawn in the last section.

II. THEORETICAL MODEL

Astrophysical S factor of the radiation capture process is expressed in terms of the cross section as [36]

$$S(E) = E \sigma(E) \exp(2\pi\eta) \quad (1)$$

where E is the collision energy in the center-of-mass (cm) frame and η is the Sommerfeld parameter. The cross section reads as [23, 36]

$$\sigma(E) = \sum_{J_f \lambda \Omega} \sigma_{J_f \lambda}(\Omega), \quad (2)$$

where $\Omega = E$ or M (electric or magnetic transition), λ is a multiplicity of the transition, J_f is the total angular momentum of the final state. For a particular final state with total momentum J_f and multiplicity λ we have

$$\begin{aligned} \sigma_{J_f \lambda}(\Omega) &= \sum_J \frac{(2J_f + 1)}{[S_1][S_2]} \frac{32\pi^2(\lambda + 1)}{\hbar\lambda([\lambda]!!)^2} k_\gamma^{2\lambda+1} C^2(S) \\ &\times \sum_{l_S} \frac{1}{k_i^2 v_i} | \langle \Psi_{l_f S}^{J_f} \| M_\lambda^\Omega \| \Psi_{l_S}^J \rangle |^2, \end{aligned} \quad (3)$$

where $\Psi_{l_S}^J$ and $\Psi_{l_f S}^{J_f}$ are the initial and final state wave functions, respectively, M_λ^Ω is the electric or magnetic transition operator, l, l_f are the orbital momenta of the initial and final states, respectively, k_i and v_i are the wave number and velocity of the α - ^3He (or α - ^3H) relative motion of the entrance channel, respectively; S_1, S_2 are spins of the clusters α and ^3He (or ^3H), $k_\gamma = E_\gamma/\hbar c$ is the wave number of the photon corresponding to energy $E_\gamma = E_{\text{th}} + E$, where E_{th} is the threshold energy. The spectroscopic factor [36] $C^2(S)$ within the potential approach is equal to 1, since the potential reproduces the two-body experimental data, energies and phase shifts in partial waves [37]. We also use short-hand notations $[S] = 2S + 1$ and $[\lambda]!! = (2\lambda + 1)!!$. Further details of the wave functions and matrix element calculations can be found in Ref. [22].

III. NUMERICAL RESULTS

A. Details of the calculations and phase-shift descriptions

We use simple Gaussian-form potentials for the $\alpha-^3\text{He}$ and $\alpha-^3\text{H}$ two-body interactions [22, 23]:

$$V^{lSj}(r) = V_0 \exp(-\alpha_0 r^2) + V_c(r), \quad (4)$$

where the Coulomb part is given as

$$V_c(r) = \begin{cases} Z_1 Z_2 e^2 / r & \text{if } r > R_c, \\ Z_1 Z_2 e^2 (3 - r^2 / R_c^2) / (2R_c) & \text{otherwise,} \end{cases} \quad (5)$$

with the Coulomb parameter R_c , and charge numbers Z_1 , Z_2 of the first and second clusters, respectively. The parameters α_0 and V_0 of the potential are specified for each partial wave. In Ref. [22] we examined several potential models for the description of the $\alpha-^3\text{He}$ and $\alpha-^3\text{H}$ interactions. As discussed in the introduction, the d-wave potentials can be further improved by modifying the depth (V_0) and width (α_0) parameters for the better description of the astrophysical S factors at intermediate energies.

The Schrödinger equation in the entrance and exit channels are solved with the $\alpha-^3\text{He}$ and $\alpha-^3\text{H}$ central potentials as defined in Eq.(4) with the corresponding Coulomb part from Eq.(5). The same entry parameter values as in Ref. [22] are used: $\hbar^2/2m_N=20.7343$ MeV fm² and $R_c=3.095$ fm (Coulomb parameter), however the nuclear masses are taken as $m_{^4\text{He}} = 4m_N$ and $m_{^3\text{He}} = m_{^3\text{H}} = 3m_N$, where m_N is the nucleon mass.

The expressions for the astrophysical S factor and cross section given above are valid only for the radial scattering wave function (the radial component of the initial state wave function Ψ_{lS}^J) normalized at large distances as

$$u_E^{(lSj)}(r) \xrightarrow{r \rightarrow \infty} \cos \delta_{lSj}(E) F_l(\eta, kr) + \sin \delta_{lSj}(E) G_l(\eta, kr), \quad (6)$$

where k is the wave number of the relative motion, F_l and G_l are regular and irregular Coulomb functions, respectively, and $\delta_{lSj}(E)$ is the phase shift in the (l, S, j) th partial wave. The scattering wave function $u_E(r)$ of the relative motion is calculated as a solution of the Schrödinger equation using the Numerov method with an appropriate potential subject to the boundary condition specified in Eq. (6).

The depth and width parameters of the α - ^3He and α - ^3H model potentials V_D^n and V_{M1}^n are given in Tables I and II, respectively. In 3th and 4th columns of the tables the energies of forbidden states are presented. The potentials contain two forbidden states in the s waves, while a single forbidden states in the each of $p_{3/2}$, $p_{1/2}$, $d_{3/2}$, $d_{5/2}$ partial waves. These potentials differ from each other only in the s and p waves. At the same time, model potentials V_D^n and V_{M1}^n are similar to potentials V_D^a and V_{M1}^a from Ref. [22], respectively. The only difference is in the d -wave parameter values. The latter have now been fitted to better reproduce the astrophysical S factors at larger energies.

TABLE I: Values of the depth (V_0) and width (α_0) parameters of the α - ^3He (^3H) potential V_D^n in different partial waves (see Eq. (4)).

L_J	V_0 (MeV)	α_0 (fm $^{-2}$)	$E_{\text{FS}}^{7\text{Be}}$ (MeV)	$E_{\text{FS}}^{7\text{Li}}$ (MeV)
$s_{1/2}$	-78.0	0.186	-40.03; -7.03	-41.34; -8.09
$p_{3/2}$	-83.8065	0.15747	-27.11	-28.33
$p_{1/2}$	-82.0237	0.15747	-26.02	-27.24
$d_{3/2}$	-180.0	0.4173	-11.96	-13.22
$d_{5/2}$	-190.0	0.4017	-18.13	-19.39
$f_{5/2}$	-75.9	0.15747	-	-
$f_{7/2}$	-85.2	0.15747	-	-

TABLE II: Values of the depth (V_0) and width (α_0) parameters of the α - ^3He (^3H) potential V_{M1}^n in different partial waves (see Eq. (4)).

L_J	V_0 (MeV)	α_0 (fm $^{-2}$)	$E_{\text{FS}}^{7\text{Be}}$ (MeV)	$E_{\text{FS}}^{7\text{Li}}$ (MeV)
$s_{1/2}$	-50.0	0.109	-25.70; -5.17	-26.95; -6.11
$p_{3/2}$	-75.59760	0.13974	-24.58	-25.78
$p_{1/2}$	-70.75751	0.13308	-22.55	-23.74
$d_{3/2}$	-180.0	0.4173	-11.96	-13.22
$d_{5/2}$	-190.0	0.4017	-18.13	-19.39
$f_{5/2}$	-75.9	0.15747	-	-
$f_{7/2}$	-85.2	0.15747	-	-

In Fig. 1 the experimental data [38] for the ${}^3\text{He} + \alpha$ (panel a) and ${}^3\text{H} + \alpha$ (panel b) d -wave scattering phase shift are compared with the theoretical calculations using the new model potentials V_D^n and V_{M1}^n . The phase shift description in the other partial waves were given in Ref. [22]. Additionally, the presented models reproduce the energy spectrum of the ${}^7\text{Be}$ and ${}^7\text{Li}$ nuclei, as well as the empirical values of the ANC for the ground $p_{3/2}$ and the first excited $p_{1/2}$ bound states of the ${}^7\text{Be}$ nucleus [22]. Indeed, the V_D^n model yields $C(3/2^-)=4.34 \text{ fm}^{-1/2}$ and $C(1/2^-)=3.71 \text{ fm}^{-1/2}$, while the alternative V_{M1}^n model reproduces the ANC values of $C(3/2^-)=4.785 \text{ fm}^{-1/2}$ and $C(1/2^-)=4.242 \text{ fm}^{-1/2}$ extracted from the analysis of the experimental data using the DWBA method [35].

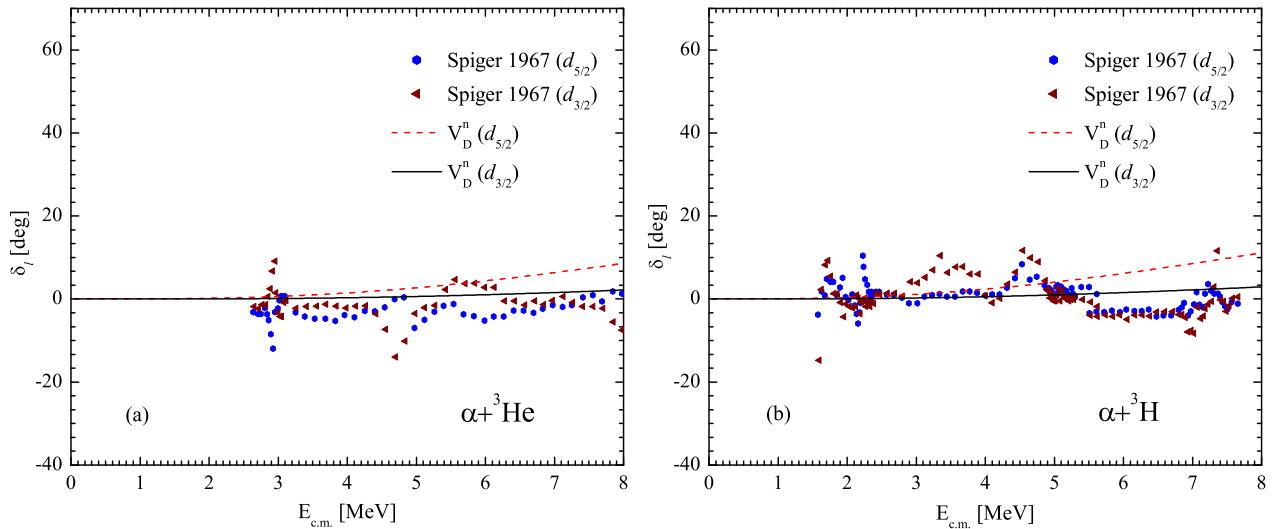


FIG. 1: d -wave phase shifts for the ${}^3\text{He} + \alpha$ (panel a) and ${}^3\text{H} + \alpha$ (panel b) scattering within potential models V_D^n and V_{M1}^n in comparison with experimental data from Ref. [38].

B. Astrophysical S factor of the ${}^3\text{He}(\alpha, \gamma){}^7\text{Be}$ reaction

For the study of the ${}^3\text{He}(\alpha, \gamma){}^7\text{Be}$ direct radiative capture process we first use the potential V_D^n . Partial E1 astrophysical S factors, estimated with the V_D^n potential are presented in Fig. 2. Panel a compares the present results for the initial d -wave contribution with the corresponding ones obtained in Ref. [22] using the potential model V_D^a . In panel b the contributions from different initial s and d partial waves are shown. As can be seen from the figure, the d -wave contribution increases significantly at larger energies.

Contributions from the E1, E2 and M1 astrophysical S factors for the ${}^3\text{He}(\alpha, \gamma){}^7\text{Be}$ direct

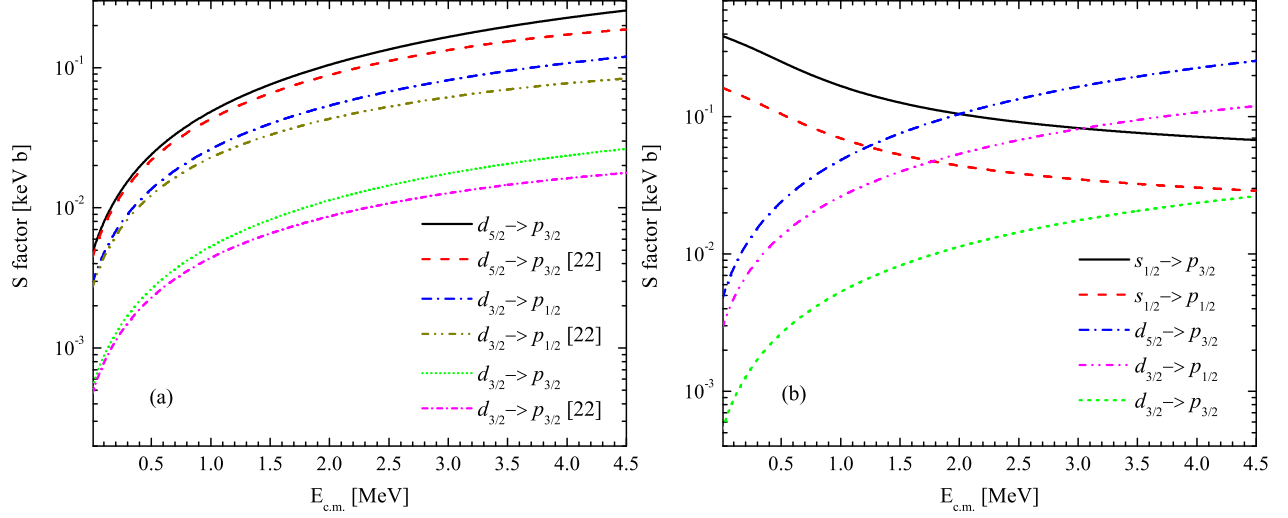


FIG. 2: Partial E1 astrophysical S factors for the ${}^3\text{He}(\alpha, \gamma){}^7\text{Be}$ capture reaction calculated with the V_D^n model potential in comparison with the results of Ref. [22].

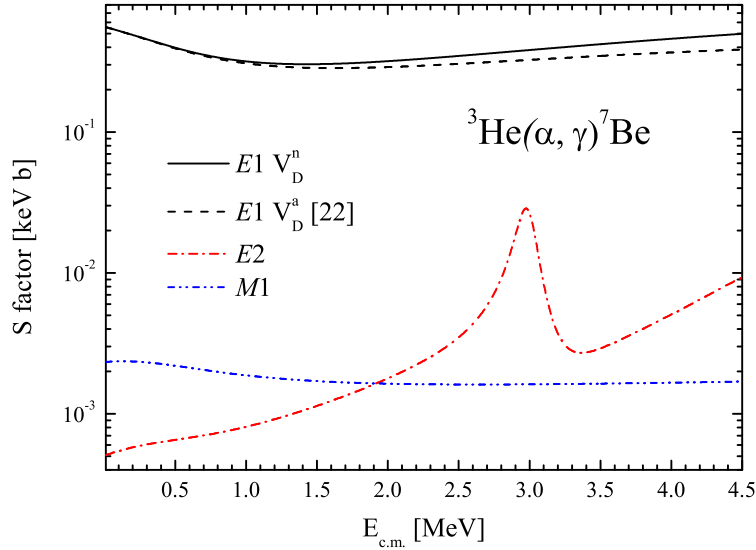


FIG. 3: E1, E2 and M1 components of the astrophysical S factors for the ${}^3\text{He}(\alpha, \gamma){}^7\text{Be}$ direct capture reaction calculated with the model potential V_D^n . The corresponding E1 component from Ref. [22] is also shown.

capture reaction calculated with the model potential V_D^n are presented in Fig. 3. As can be seen from the figure, modification of the potential in d waves significantly increases the astrophysical S factor in comparison with the results of Ref. [22] at energies above 0.5 MeV.

Figure 4 compares the astrophysical S factors calculated with modified potentials V_D^n

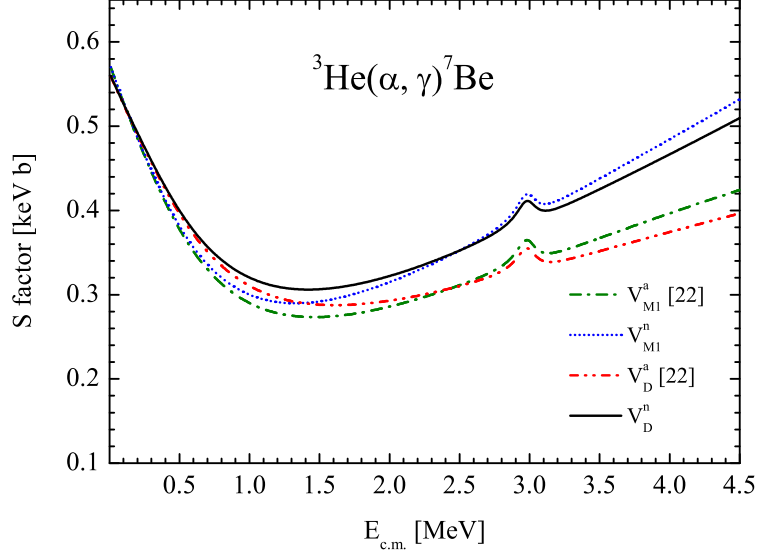


FIG. 4: Astrophysical S factor for the ${}^3\text{He}(\alpha, \gamma){}^7\text{Be}$ direct capture reaction calculated with modified potentials V_D^n and V_{M1}^n in comparison with experimental data from Refs. [16–21, 46–49] and the results of Ref. [22].

and V_{M1}^n with experimental data from Refs. [16–21, 46–49] and the results of Ref. [22]. A substantial improvement is achieved within the new models V_D^n and V_{M1}^n at energies around and above the resonance energy.

In Fig. 5 the final results for the astrophysical S factors of the ${}^3\text{He}(\alpha, \gamma){}^7\text{Be}$ direct capture reaction are compared with the available data and results of *ab-initio* calculations from Refs. [32, 33]. As can be seen from the figure, the potential models V_D^n and V_{M1}^n describe both absolute values and energy dependence of the experimental data for the astrophysical S factor in a wide energy region from tens of keV to a few MeV.

C. Astrophysical S factor of the ${}^3\text{H}(\alpha, \gamma){}^7\text{Li}$

As noted in the Introduction, the same model potentials V_D^n and V_{M1}^n are applied for the study of the mirror capture reaction ${}^3\text{H}(\alpha, \gamma){}^7\text{Li}$. The Coulomb part of these potentials, defined in Eq. (5), is modified according to the charge value of the ${}^3\text{H}$ cluster, $Z=1$. As demonstrated in Fig. 1 (panel b), the phase shifts in the $d_{3/2}$ and $d_{5/2}$ partial waves are well described. The binding energies $E_b(3/2^-)=2.467$ MeV and $E_b(1/2^-)=1.990$ MeV of the bound states have been reproduced in Ref. [22].

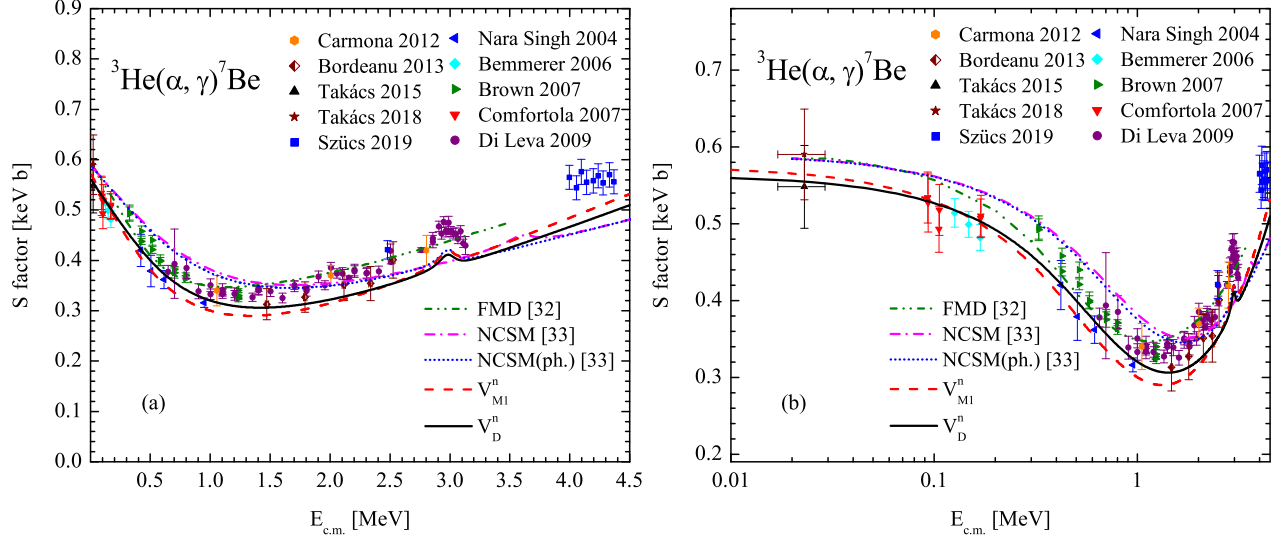


FIG. 5: (a) Astrophysical S factor for the ${}^3\text{He}(\alpha, \gamma){}^7\text{Be}$ direct capture reaction calculated with modified potential models V_D^n and V_{M1}^n in comparison with experimental data from Refs. [16–21, 46–49] and *ab-initio* calculations from Refs. [32, 33]. Panel (b) highlights the low-energy region.

In Fig. 6 we compare the contributions of the $E1$, $E2$ and $M1$ astrophysical S factors for the ${}^3\text{H}(\alpha, \gamma){}^7\text{Li}$ direct capture reaction calculated with the potentials V_D^n and V_D^a from Ref. [22]. As in the case of ${}^7\text{Be}$, the relative contribution of the $E1$ transition increases with the energy in comparison with the results of Ref. [22].

Figure 7 presents the astrophysical S factor for the ${}^3\text{H}(\alpha, \gamma){}^7\text{Li}$ direct capture reaction calculated with modified potentials V_D^n and V_{M1}^n in comparison with experimental data from Refs. [39–45] and the results of Ref. [22]. An increase of the astrophysical S factor within the models V_D^n and V_{M1}^n is seen for energies $E > 0.5$ MeV. The best description of the data is obtained within the V_{M1}^n model.

In Fig. 8 the astrophysical S factors for the ${}^3\text{H}(\alpha, \gamma){}^7\text{Li}$ direct capture reaction calculated with modified potential models V_D^n and V_{M1}^n are compared with available experimental data and *ab-initio* calculations. As can be seen, the best description of the data for both absolute value and energy dependence of the astrophysical S factor is obtained with the new potential models V_D^n and V_{M1}^n . As noted above, all the parameters of the model potentials have been adjusted to the data for the ${}^7\text{Be}$ nucleus. With that the results for the astrophysical S factor for the mirror ${}^7\text{Li}$ nucleus are obtained without any fitting parameters. Additionally, the

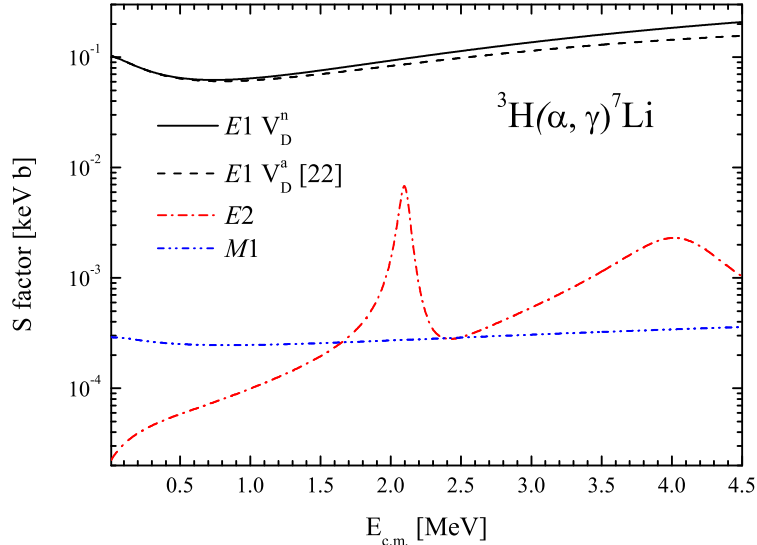


FIG. 6: Comparison of contributions of the E1, E2 and M1 astrophysical S factors for the ${}^3\text{H}(\alpha, \gamma){}^7\text{Li}$ direct capture reaction calculated with modified potential model V_D^n compared with the results of Ref. [22].

same potentials describe the binding energies and phase shifts for the mirror ${}^7\text{Li}$ nucleus [22].

IV. REACTION RATES AND PRIMORDIAL ABUNDANCE OF THE ${}^7\text{Li}$ ELEMENT

A. Estimation of reaction rates for the ${}^3\text{He}(\alpha, \gamma){}^7\text{Be}$ process

In Table III estimated values for the reaction rate are given for the ${}^3\text{He}(\alpha, \gamma){}^7\text{Be}$ direct capture process in the temperature interval $10^6 \text{ K} \leq T \leq 10^9 \text{ K}$ ($0.001 \leq T_9 \leq 1$). From the values presented in the table one can conclude that the numerical results for the models V_D^n and V_{M1}^n are in a good agreement with those obtained using the models V_D^a and V_{M1}^a [50], respectively.

In Fig. 9 we present estimated reaction rates for the direct ${}^3\text{He}(\alpha, \gamma){}^7\text{Be}$ capture process within the modified potential models V_D^n and V_{M1}^n , normalized to the standard NACRE 1999 experimental data [36]. For comparison we also display the lines corresponding to the results of Refs. [18, 51, 52] and more recent NACRE II 2013 data [53]. As can be seen from the figure, the potential model results lie between the lines for the microscopic R-matrix approach from Ref.[52] and the NACRE II data. Other models [18, 51] overestimate the

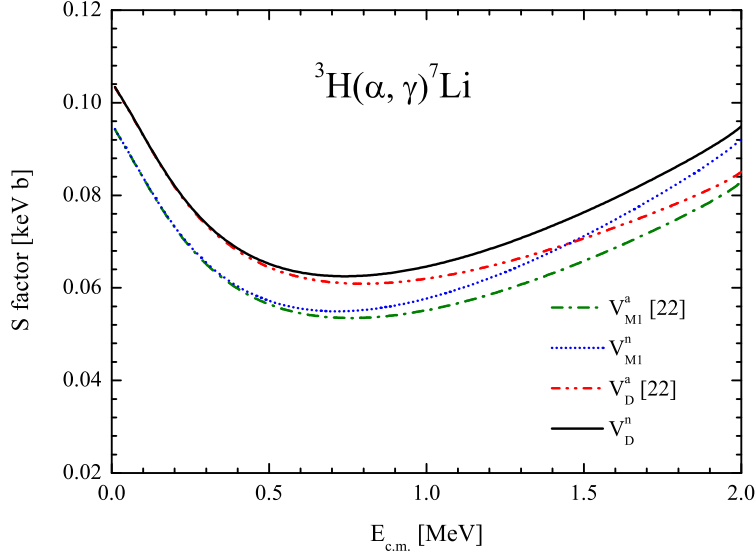


FIG. 7: Astrophysical S factor for the ${}^3\text{H}(\alpha, \gamma){}^7\text{Li}$ direct capture reaction calculated with modified potential models V_D^n and V_{M1}^n in comparison with available experimental data from Refs. [39–45] and the results of Ref. [22].

NACRE II data.

In order to estimate the primordial abundance of the ${}^7\text{Li}$ element the well known PARthENoPE [54] public code is employed. It operates with an analytical form of the reaction rate dependence on the temperature T_9 . For this reason the theoretical reaction rates from Table III are approximated (within an uncertainty of 0.971% for the V_D^n and 0.582% for the V_{M1}^n) by the analytical form

$$N_A(\sigma v) = p_0 T_9^{-2/3} \exp(-C_0 T_9^{-1/3}) \times (1 + p_1 T_9^{1/3} + p_2 T_9^{2/3} + p_3 T_9 + p_4 T_9^{4/3} + p_5 T_9^{5/3}) + p_6 T_9^{-3/2} \exp(-C_{01} T_9^{-1}). \quad (7)$$

The coefficients of the analytical polynomial approximation of the ${}^3\text{He}(\alpha, \gamma){}^7\text{Be}$ reaction rates estimated within the potential models V_{M1}^n and V_D^n are given in Table IV in the temperature interval $0.001 \leq T_9 \leq 1$. In addition, for this process the other coefficients are $C_0 = 12.813$ and $C_{01} = 15.889$.

On the basis of the theoretical reaction rates and with the help of the PARthENoPE [54] code we have estimated a contribution from the ${}^3\text{He}(\alpha, \gamma){}^7\text{Be}$ direct capture reaction to the primordial abundance of the ${}^7\text{Li}$ element. If we adopt the Planck 2015 best fit for the baryon density parameter $\Omega_b h^2 = 0.02229_{-0.00027}^{+0.00029}$ [55] and the neutron life time $\tau_n = 880.2 \pm 1.0$

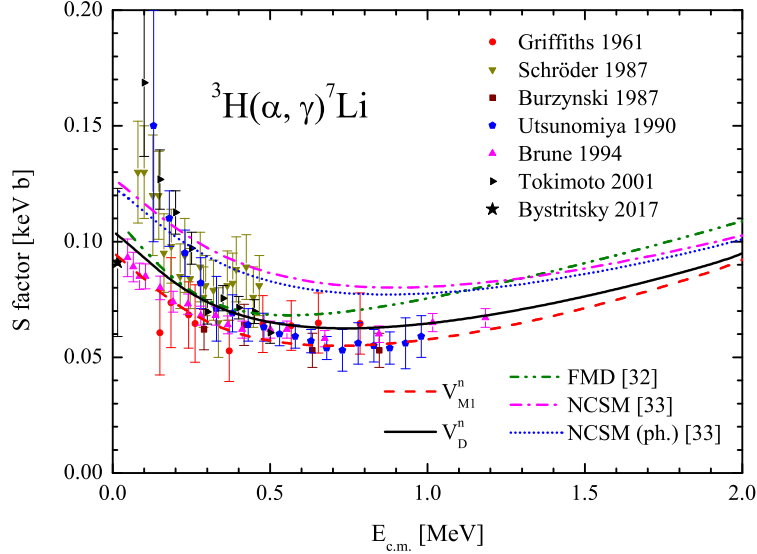


FIG. 8: (a) Astrophysical S factor for the ${}^3\text{H}(\alpha, \gamma){}^7\text{Li}$ direct capture reaction calculated with modified potential models V_D^n and V_{M1}^n in comparison with available experimental data from Refs. [39–45] and *ab-initio* calculations [32, 33]. Panel (b) highlights the low-energy region.

s [56], for the ${}^7\text{Li}/\text{H}$ abundance ratio we have an estimate $(4.930 \pm 0.129) \times 10^{-10}$ within potential model V_D^n and the estimate $(4.842 \pm 0.126) \times 10^{-10}$ within the model V_{M1}^n which agree well, within 2%, to be specific. As discussed below, these numbers barely change the ${}^7\text{Li}/\text{H}$ abundance ratio if the contribution from the ${}^3\text{H}(\alpha, \gamma){}^7\text{Li}$ direct capture reaction is included.

B. Estimation of reaction rates for the ${}^3\text{H}(\alpha, \gamma){}^7\text{Li}$ direct capture process

In Table V we give theoretical estimations for the ${}^3\text{H}(\alpha, \gamma){}^7\text{Li}$ direct capture reaction rates in the temperature interval $10^6 \text{ K} \leq T \leq 10^9 \text{ K}$ ($0.001 \leq T_9 \leq 1$) calculated with the same modified potential models V_{M1}^n and V_D^n which have been used for the ${}^3\text{He}(\alpha, \gamma){}^7\text{Be}$ process. Figure 10 displays these results normalized to the standard NACRE 1999 experimental data [36]. For the comparison we also display the lines corresponding to the results of the microscopic R-matrix method [52] and new NACRE II 2013 data [53].

The coefficients of the analytical polynomial approximation of the ${}^3\text{H}(\alpha, \gamma){}^7\text{Li}$ reaction rates estimated within the potential models V_{M1}^n and V_D^n are given in Table VI in the temperature interval $0.001 \leq T_9 \leq 1$. The remaining coefficients are $C_0 = 8.072$ and $C_{01} = 3.689$.

TABLE III: Theoretical estimates of the reaction rates for the direct ${}^3\text{He}(\alpha, \gamma){}^7\text{Be}$ capture process in the temperature interval $10^6 \text{ K} \leq T \leq 10^9 \text{ K}$ ($0.001 \leq T_9 \leq 1$)

T_9	V_{M1}^n	V_D^n	T_9	V_{M1}^n	V_D^n
0.001	9.554×10^{-48}	9.367×10^{-48}	0.070	9.755×10^{-7}	9.662×10^{-7}
0.002	1.949×10^{-36}	1.911×10^{-36}	0.080	3.450×10^{-6}	3.421×10^{-6}
0.003	5.896×10^{-31}	5.784×10^{-31}	0.090	1.001×10^{-5}	9.932×10^{-6}
0.004	1.677×10^{-27}	1.645×10^{-27}	0.100	2.498×10^{-5}	2.481×10^{-5}
0.005	4.775×10^{-25}	4.687×10^{-25}	0.110	5.545×10^{-5}	5.514×10^{-5}
0.006	3.547×10^{-23}	3.482×10^{-23}	0.120	1.121×10^{-4}	1.116×10^{-4}
0.007	1.104×10^{-21}	1.084×10^{-21}	0.130	2.102×10^{-4}	2.093×10^{-4}
0.008	1.877×10^{-20}	1.844×10^{-20}	0.140	3.699×10^{-4}	3.687×10^{-4}
0.009	2.057×10^{-19}	2.021×10^{-19}	0.150	6.175×10^{-4}	6.161×10^{-4}
0.010	1.615×10^{-18}	1.586×10^{-18}	0.160	9.856×10^{-4}	9.842×10^{-4}
0.011	9.773×10^{-18}	9.604×10^{-18}	0.180	2.249×10^{-3}	2.249×10^{-3}
0.012	4.805×10^{-17}	4.723×10^{-17}	0.200	4.562×10^{-3}	4.569×10^{-3}
0.013	1.995×10^{-16}	1.961×10^{-16}	0.250	1.864×10^{-2}	1.874×10^{-2}
0.014	7.196×10^{-16}	7.076×10^{-16}	0.300	5.401×10^{-2}	5.446×10^{-2}
0.015	2.307×10^{-15}	2.269×10^{-15}	0.350	1.254×10^{-1}	1.268×10^{-1}
0.016	6.694×10^{-15}	6.584×10^{-15}	0.400	2.496×10^{-1}	2.531×10^{-1}
0.018	4.400×10^{-14}	4.329×10^{-14}	0.450	4.447×10^{-1}	4.522×10^{-1}
0.020	2.224×10^{-13}	2.189×10^{-13}	0.500	7.286×10^{-1}	7.426×10^{-1}
0.025	5.683×10^{-12}	5.598×10^{-12}	0.600	1.630×10^0	1.668×10^0
0.030	6.692×10^{-11}	6.597×10^{-11}	0.700	3.072×10^0	3.157×10^0
0.040	2.408×10^{-9}	2.377×10^{-9}	0.800	5.150×10^0	5.312×10^0
0.050	3.049×10^{-8}	3.014×10^{-8}	0.900	7.929×10^0	8.204×10^0
0.060	2.100×10^{-7}	2.078×10^{-7}	1.000	1.145×10^1	1.189×10^1

In this case, the analytical formula (7) with the parameter values from Table VI reproduces the theoretical reaction rates from Table V (within an uncertainty 0.599% for V_D^n and 0.647% for V_{M1}^n).

TABLE IV: Fitted values of the coefficients of analytical approximation for the direct capture reaction ${}^3\text{He}(\alpha, \gamma){}^7\text{Be}$

Model	p_0	p_1	p_2	p_3	p_4	p_5	p_6
V_{M1}^n	2.697×10^6	8.105	-26.574	42.958	-35.272	11.347	446.257
V_D^n	2.636×10^6	8.155	-26.704	43.602	-35.987	11.595	465.678

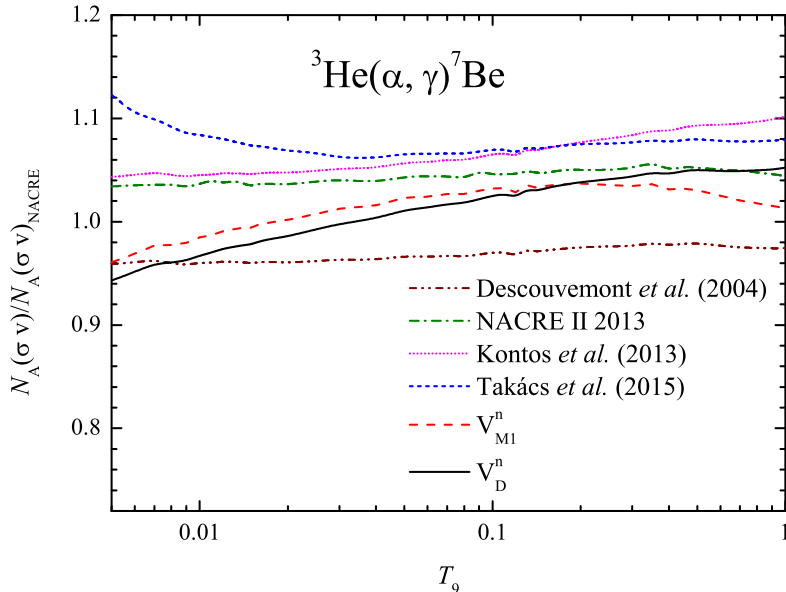


FIG. 9: Reaction rates of the ${}^3\text{He}(\alpha, \gamma){}^7\text{Be}$ direct capture process normalized to the NACRE 1999 experimental data in comparison with results from Refs.[18, 51, 52] and more recent NACRE II 2013 data [53].

Now including the obtained theoretical reaction rates for both ${}^3\text{He}(\alpha, \gamma){}^7\text{Be}$ and ${}^3\text{H}(\alpha, \gamma){}^7\text{Li}$ capture processes into the nuclear reaction network with the help of the PARthENoPE [54] code, we can evaluate the primordial abundance of the ${}^7\text{Li}$ element. Adopting the aforementioned values of the baryon density and the neutron life time, for the ${}^7\text{Li}/\text{H}$ abundance ratio we have an estimate $(4.936 \pm 0.129) \times 10^{-10}$ within the model V_D^n , while the model V_{M1}^n yields $(4.835 \pm 0.127) \times 10^{-10}$ [50]. These numbers are slightly different than the corresponding estimates based exclusively on the ${}^3\text{He}(\alpha, \gamma){}^7\text{Be}$ process.

TABLE V: Theoretical estimates of the reaction rates for the ${}^3\text{H}(\alpha, \gamma){}^7\text{Li}$ direct capture process in the temperature interval $10^6 \text{ K} \leq T \leq 10^9 \text{ K}$ ($0.001 \leq T_9 \leq 1$)

T_9	V_{M1}^n	V_D^n	T_9	V_{M1}^n	V_D^n
0.001	5.595×10^{-28}	6.130×10^{-28}	0.070	1.326×10^{-2}	1.461×10^{-2}
0.002	6.285×10^{-21}	6.887×10^{-21}	0.080	2.839×10^{-2}	3.130×10^{-2}
0.003	1.613×10^{-17}	1.767×10^{-17}	0.090	5.384×10^{-2}	5.939×10^{-2}
0.004	2.252×10^{-15}	2.468×10^{-15}	0.100	9.318×10^{-2}	1.028×10^{-1}
0.005	7.497×10^{-14}	8.219×10^{-14}	0.110	1.502×10^{-1}	1.658×10^{-1}
0.006	1.081×10^{-12}	1.185×10^{-12}	0.120	2.286×10^{-1}	2.525×10^{-1}
0.007	9.075×10^{-12}	9.951×10^{-12}	0.130	3.324×10^{-1}	3.673×10^{-1}
0.008	5.234×10^{-11}	5.740×10^{-11}	0.140	4.651×10^{-1}	5.142×10^{-1}
0.009	2.297×10^{-10}	2.519×10^{-10}	0.150	6.304×10^{-1}	6.973×10^{-1}
0.010	8.194×10^{-10}	8.989×10^{-10}	0.160	8.316×10^{-1}	9.201×10^{-1}
0.011	2.488×10^{-9}	2.729×10^{-9}	0.180	1.353×10^0	1.499×10^0
0.012	6.641×10^{-9}	7.286×10^{-9}	0.200	2.052×10^0	2.274×10^0
0.013	1.596×10^{-8}	1.751×10^{-8}	0.250	4.677×10^0	5.191×10^0
0.014	3.516×10^{-8}	3.858×10^{-8}	0.300	8.672×10^0	9.640×10^0
0.015	7.201×10^{-8}	7.903×10^{-8}	0.350	1.409×10^1	1.568×10^1
0.016	1.386×10^{-7}	1.521×10^{-7}	0.400	2.091×10^1	2.330×10^1
0.018	4.408×10^{-7}	4.839×10^{-7}	0.450	2.905×10^1	3.242×10^1
0.020	1.191×10^{-6}	1.308×10^{-6}	0.500	3.843×10^1	4.293×10^1
0.025	8.679×10^{-6}	9.534×10^{-6}	0.600	6.045×10^1	6.767×10^1
0.030	3.920×10^{-5}	4.308×10^{-5}	0.700	8.615×10^1	9.661×10^1
0.040	3.484×10^{-4}	3.832×10^{-4}	0.800	1.148×10^2	1.289×10^2
0.050	1.629×10^{-3}	1.793×10^{-3}	0.900	1.457×10^2	1.638×10^2
0.060	5.244×10^{-3}	5.775×10^{-3}	1.000	1.783×10^2	2.008×10^2

V. CONCLUSIONS

The astrophysical ${}^3\text{He}(\alpha, \gamma){}^7\text{Be}$ and ${}^3\text{H}(\alpha, \gamma){}^7\text{Li}$ direct capture reactions have been studied in an updated two-body potential model. The parameters of the central potentials of

TABLE VI: Fitted values of the coefficients of analytical approximation for the ${}^3\text{H}(\alpha, \gamma){}^7\text{Li}$ direct capture reaction

Model	p_0	p_1	p_2	p_3	p_4	p_5	p_6
V_{M1}^n	4.948×10^5	4.053	-13.252	21.105	-17.624	5.868	47.365
V_D^n	5.422×10^5	4.042	-13.159	21.080	-17.681	5.899	53.267

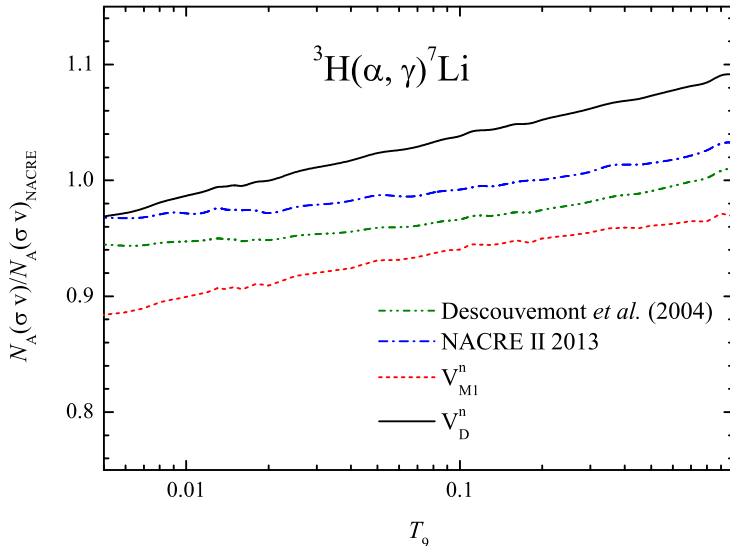


FIG. 10: Reaction rates of the direct ${}^3\text{H}(\alpha, \gamma){}^7\text{Li}$ capture process normalized to the NACRE 1999 experimental data [36] in comparison with the results of Ref.[52] and new NACRE II 2013 data [53]

a simple Gaussian form have been adjusted to reproduce the $\alpha+{}^3\text{He}$ phase shifts in the s , p , d and f partial waves and the binding energies of the ${}^7\text{Be}$ ground $3/2^-$ and first excited $1/2^-$ states. At the same time, properties of the mirror ${}^7\text{Li}$ nucleus, phase shifts in the partial waves and the binding energies of the ground $3/2^-$ and first excited $1/2^-$ states are reproduced without any additional adjustment parameters.

It is found that due to the dominance of the E1 transition in the capture processes, there is a possibility to adjust the parameters of the potential in the initial s - and d -waves in order to optimize the description of the astrophysical S factor at low and intermediate energy regions, respectively.

In conclusion, the potential models V_{M1}^n , V_D^n have been suggested for the description of the $\alpha + {}^3\text{H}$ and $\alpha + {}^3\text{He}$ interactions. These models reproduce spectroscopic properties and

phase shifts of both ${}^7\text{Be}$ and ${}^7\text{Be}$ nuclei. They describe well the experimental data for the astrophysical S factor of the capture process ${}^3\text{He}(\alpha, \gamma){}^7\text{Be}$ in a wide energy region, extending to 4.5 MeV. This includes the new data of the LUNA collaboration around 100 keV and the latest data at the Gamov peak obtained on the basis of the observed neutrino fluxes from the Sun, $S_{34}(23_{-5}^{+6} \text{ keV})=0.548\pm 0.054 \text{ keV b}$. The same potentials describe the astrophysical S factor for the mirror capture reaction ${}^3\text{H}(\alpha, \gamma){}^7\text{Li}$ with a good accuracy.

The calculated values of the astrophysical S factors and reaction rates for the ${}^3\text{He}(\alpha, \gamma){}^7\text{Be}$ and ${}^3\text{H}(\alpha, \gamma){}^7\text{Li}$ direct capture reactions are in good agreement with the results of microscopic models and *ab-initio* calculations. For the primordial abundance of the ${}^7\text{Li}$ element an estimate $(4.89 \pm 0.18) \times 10^{-10}$ have been obtained. This result is within the range of the standard BBN model estimates.

Acknowledgements

We thank J. Dohet-Eraly for providing us with the results of Ref. [33] for the astrophysical S factor in a tabulated form. A.S.K. acknowledges the support from the Australian Research Council.

-
- [1] L. Sbordone, P. Bonifacio, E. Caffau, *Astron. and Astrophys.* **522** (2010) A26
 - [2] R.H. Cyburt, B.D. Fields, K.A. Olive and T-H. Yeh, *Reviews of Modern Physics* **88**, 1 (2016)
 - [3] LUNA Collaboration (D. Trezzi, *et al.*) *Astropart. Phys.* **89** 57 (2017)
 - [4] M. Asplund, *et al.*, *Astrophys. J.* **644** (2006) 229.
 - [5] Proc. of Inter Conf. "Lithium in the universe: to be or not to be? Monte Porzio Catone, November 18-22, 2019 Editors: G. Cescutti, A. Korn and P. Ventura". MEMORIE DELLA SOCIETA ASTRONOMICA ITALIANA Vol. 91 (2020), pp. 1-179.
 - [6] E.M. Tursunov, A.S. Kadyrov, S.A. Turakulov, I. Bray, *Phys. Rev. C* **94** (2016) 015801.
 - [7] D. Baye, E.M. Tursunov, *J. Phys. G, Nucl. Part. Phys.* **45** (2018) 085102.
 - [8] E.M. Tursunov, S.A. Turakulov, A.S. Kadyrov, I. Bray, *Phys. Rev. C* **98** (2018) 055803.
 - [9] E.M. Tursunov, S.A. Turakulov, A.S. Kadyrov, *Nucl. Phys.* **A1000** (2020) 121884
 - [10] LUNA Collaboration (M. Anders, *et al.*) *Phys. Rev. Lett.* **113**, 042501 (2014).

- [11] E.M. Tursunov, S.A. Turakulov, P. Descouvemont, Phys. At. Nucl. **78** (2015) 193.
- [12] E. G. Adelberger *et al.*, Rev. Mod. Phys. **83**, 195 (2011).
- [13] B. D. Fields, Ann. Rev. Nucl. Particle Sci. **61** (2011) 47.
- [14] A. Serenelli, C. Peña-Garay, and W. C. Haxton, Phys. Rev. D **87**, 043001 (2013).
- [15] A. Coc and E. Vangioni, Int. J. Mod. Phys. E **26**, 1741002 (2017).
- [16] D. Bemmerer, F. Confortola, H. Costantini, A. Formicola, Gy. Gyürky, *et al.*, Phys. Rev. Lett. **97**, 122502 (2006).
- [17] F. Confortola, D. Bemmerer, H. Costantini, A. Formicola, Gy. Gyürky, *et al.*, Phys. Rev. C **75**, 065803 (2007).
- [18] M.P. Takács, D. Bemmerer, T. Szücs, and K. Zuber, Phys. Rev. D **91**, 123526 (2015).
- [19] M.P. Takács, D. Bemmerer, A.R. Junghans, K. Zuber, Nucl. Phys. A **970**, 78 (2018).
- [20] C. Bordeanu, Gy. Gyürky, Z. Halász, T. Szücs, G. G. Kiss, Z. Elekes, J. Farkas, Zs. Fülöp, and E. Somorjai, Nucl. Phys. A **908**, 1 (2013).
- [21] T. Szücs, G.G. Kiss, Gy. Gyürky, Z. Halász, T. N. Szegedi, Zs. Fülöp, Phys. Rev. C **99**, 055804 (2019).
- [22] E.M. Tursunov, S.A. Turakulov and A.S. Kadyrov, Phys. Rev. C **97**, 035802 (2018).
- [23] S.B. Dubovichenko, Physics of Atomic Nuclei, **73**, 1526 (2010).
- [24] P. Mohr, Phys. Rev. C **79**, 065804 (2009).
- [25] A. Mason, R. Chatterjee, L. Fortunato, and A. Vitturi, Eur. Phys. J. A **39**, 107 (2009).
- [26] T. Kajino, Astrophysics J. **319**, 531 (1987).
- [27] V. S. Vasilevsky, A. V. Nesterov, and T. P. Kovalenko, Physics of Atomic Nuclei, **75**, 818 (2012).
- [28] A.S. Solovyev, S.Yu. Igashov, Yu.M. Tchuvilsky, J. Phys. CS **569**, 0122020 (2014).
- [29] A.S. Solovyev, S.Yu. Igashov, Phys. Rev. C **99**, 054618 (2019).
- [30] P. Descouvemont and D. Baye, Rep. Prog. Phys. **73**, 036301 (2010).
- [31] K.M. Nollett, Phys. Rev. C **63**, 054002 (2001).
- [32] T. Neff, Phys. Rev. Lett. **106**, 042502 (2011).
- [33] J. Dohet-Eraly, P. Navratil, S. Quaglioni, W. Horiuchi, G. Hupin and F. Raimondi, Phys. Lett. B **757**, 430 (2016).
- [34] M. Vorabbi, P. Navratil, S. Quaglioni, G. Hupin, Phys. Rev. C **100**, 024304 (2019).
- [35] R. Yarmukhamedov, O.R. Tojiboev, and S.V. Artemov, Nuovo Cimento C **39**, 364 (2016).

- [36] NACRE (C. Angulo *et al.*), Nucl. Phys. A **656**, 3 (1999).
- [37] A.M. Mukhamedzhanov, Shubhchintak, and C.A. Bertulani, Phys. Rev. C **93**, 045805 (2016).
- [38] R.J. Spiger and T.A. Tombrello, Phys.Rev. **163**, 964 (1967)
- [39] G. M. Griffiths, R. A. Morrow, P. J. Riley, and J. B. Warren, Can. J. Phys. **39**, 1397 (1961).
- [40] U. Schröder, A. Redder, C. Rolfs, R. E. Azuma, L. Buchmann, C. Campbell, J. D. King, and T. R. Donoghue, Phys. Lett. B **192**, 55 (1987).
- [41] S. Burzyński, K. Czerski, A. Marcinkowski, and P. Zupranski, Nucl. Phys. A **473**, 179(1987).
- [42] H. Utsunomiya, Y.-W. Lui, *et al.*, Phys.Rev.Lett. **65**, 847 (1990).
- [43] C. R. Brune, R.W. Kavanagh, and C. Rolfs, Phys. Rev. C **50**, 2205 (1994).
- [44] Y. Tokimoto, H. Utsunomiya, *et al.*, Phys. Rev. C **63**, 035801 (2001).
- [45] V. M. Bystritsky, G. N. Dudkin, E. G. Emets, M. Filipowicz, A. R. Krylov, B. A. Nechaev, A. Nurkin, V. N. Padalko, A. V. Philippov, and A. B. Sadovsky, Phys. Part. Nucl. Lett. **14**, 560 (2017)
- [46] B. S. Nara Singh, M. Hass, Y. Nir-El, and G. Haquin, Phys. Rev. Lett. **93**, 262503 (2004).
- [47] T.A.D. Brown, C. Bordeanu, K. A. Snover, D. W. Storm, D. Melconian, A. L. Sallaska, S. K. L. Sjue, and S. Triambak, Phys. Rev. C **76**, 055801 (2007).
- [48] A. Di Leva, L. Gialanella, R. Kunz, D. Rogalla, D. Schürmann, *et al.*, Phys. Rev. Lett. **102**, 232502 (2009).
- [49] M. Carmona-Gallardo, B. S. Nara Singh, M. J. G. Borge, J. A. Briz, M. Cubero, *et al.*, Phys. Rev. C **86**, 032801 (2012).
- [50] S.A. Turakulov, E.M. Tursunov, Int. J. Mod. Phys: Conf. Ser. **49**, 1960014 (2019).
- [51] A. Kontos, E. Uberseder, R. deBoer, J. Görres, C. Akers, A. Best, M. Couder, M. Wiescher, Phys. Rev. C **87**, 065804 (2013).
- [52] P. Descouvemont, A. Adahchour, C. Angulo, A. Coc and E. Vangione-Flam, Atomic Data and Nuclear Data Tables **88**, 203 (2004)
- [53] NACRE II (Y. Xu *et al.*), Nucl. Phys. A **918**, 61 (2013).
- [54] O. Pisanti, A. Cirillo, S. Esposito, F. Iocco, G. Mangano, G. Miele, and P. D. Serpico, Comput. Phys. Commun. **178**, 956 (2008).
- [55] Planck Collaboration (P. A. R. Ade *et al.*), Astron. Astrophys. **594**, A13 (2016).
- [56] M. Tanabashi *et al.* (Particle Data Group), Phys. Rev. **D98**, 030001 (2018)
- [57] P. R. Fraser, K. Massen-Hane, A.S. Kadyrov, K. Amos, I. Bray, and L. Canton, Phys. Rev.

C **96**, 014619 (2017).

[58] W.R. Boykin, S.D. Baker, D.M. Hardy, Nucl. Phys. A **195**, 241 (1972).

[59] D.M. Hardy, R.J. Spiger, S.D. Baker, Y.S. Chen, T.A. Tombrello, Nucl. Phys. A **195**, 250 (1972).